Journal of the Korean Physical Society, Vol. 56, No. 1, January 2010, pp. 255∼261

High-speed High-resolution Terahertz Spectrometers

Youngchan Kim and Dae-Su Yee*
Center for Safety Measurement, Korea Research Institute of Standards and Science, Daejeon 305-340

Minwoo Yi and Jaewook Ahn
Department of Physics, Korea Advanced Institute of Science and Technology, Daejeon 305-701

(Received 12 January 2009, in final form 2 April 2009)

We demonstrate and characterize both asynchronous optical sampling terahertz time-domain spectroscopy (AOS THz-TDS) and terahertz frequency comb spectroscopy (TFCS) as high-speed, high-resolution terahertz (THz) spectroscopy. Two mode-locked femtosecond (fs) lasers with slightly different repetition frequencies are used without a mechanical delay stage to generate and detect THz pulses. The repetition frequencies of the two fs lasers are stabilized by use of two phase-locked loops sharing the same reference oscillator. For AOS THz-TDS, the difference frequency between the repetition frequencies is optimized, and the signal-to-noise ratio is measured as a function of the measurement time. The spectra of a THz frequency comb and its individual modes are measured using TFCS. A spectral resolution of 100 MHz is obtained in both types of spectroscopy.

PACS numbers: 07.57.Pt, 07.57.Hm
Keywords: Terahertz, Terahertz time-domain spectroscopy, Asynchronous optical sampling, Terahertz frequency comb
DOI: 10.3938/jkps.56.255

I. INTRODUCTION

The terahertz (THz) electromagnetic wave has drawn much attention due to the technological development of THz sources and detectors [1–6]. Since the THz region, generally defined as 0.1 - 10 THz, spans the range of low-energy excitations in electronic materials [7] and vibrational and rotational transitions in molecules [8], it is a key spectral region for probing fundamental physical interactions, as well as for practical applications. Also, bio-samples such as DNA films [9] and quantum systems such as Rydberg atoms [10] and semiconductor nanostructures [11] can be investigated using THz waves.

Terahertz time-domain spectroscopy (THz-TDS) using a coherent measurement method is one of the basic measurement tools in the THz field. A trade-off between frequency resolution and measurement time exists in conventional THz-TDS utilizing a single mode-locked fs laser because frequency resolution is inversely proportional to the overall time window. Generally, translational stages need a measurement time of several minutes whereas they enable a time delay scan up to hundreds of picoseconds. Contrarily, vibrating mirrors have a scan rate of up to 100 Hz while the measured time window is limited to less than 100 ps. Also, different types of optical delay lines have been devised for rapid data acquisition or high spectral resolution [12,13]. Recently, asynchronous optical sampling (AOS) has been proposed to be applied to THz-TDS to eliminate the trade-off [14–17], which should employ two fs lasers with slightly different repetition frequencies for THz wave generation and detection, respectively. AOS has been effectively applied to THz-TDS to achieve rapid data acquisition and a high spectral resolution.

Frequency comb technology emerged in the fields of optical metrology and spectroscopy in 2000. Also, terahertz frequency comb spectroscopy (TFCS) has been recently demonstrated through generation and detection of a THz frequency comb [18,19]. The THz frequency comb has many attractive features for frequency metrology, such as high accuracy, broadband selectivity, and ultranarrow linewidth. Furthermore, it can be used as a precise ruler in the frequency domain because it is extended to the THz region with no offset frequency. Thus, TFCS can be an effective tool for identifying interesting molecules with fingerprints in the THz range.

In this paper, we demonstrate, characterize, and compare the two types of high-speed high-resolution THz spectroscopy: AOS THz-TDS and TFCS. In Section II, the principles of operation for AOS THz-TDS and TFCS are explained. Section III describes our experimental setups to implement the two types of THz spectroscopy. We analyze and discuss experimental results obtained from the spectrometers in Section IV, and Section V

*E-mail: dsyee@kriss.re.kr; Fax: +82-42-868-5639

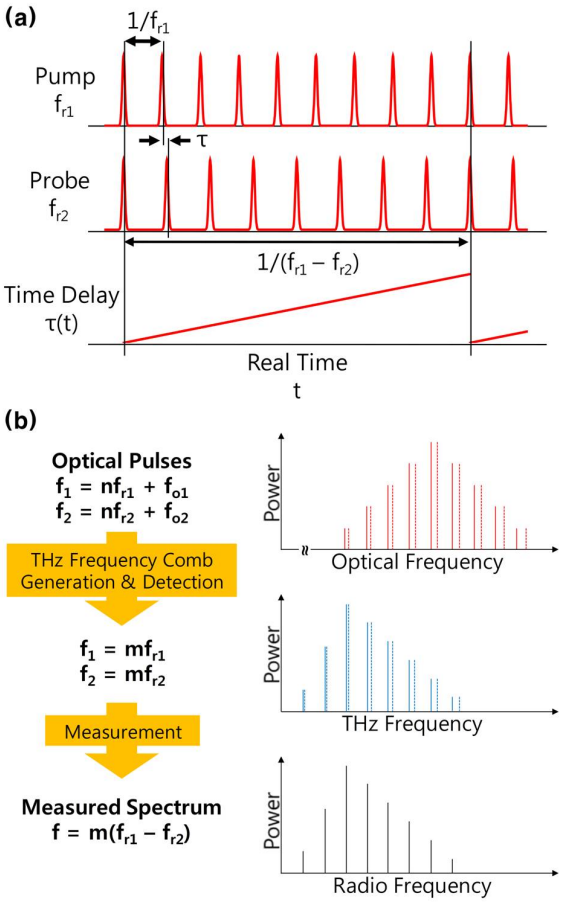

Fig. 1. (a) Illustration of the principle of the AOS THz-TDS in the time-domain. (b) Illustration of the principle of the TFCS in the frequency domain.

summarizes this paper.

II. PRINCIPLES OF OPERATION

1. AOS THz-TDS

The conventional THz-TDS utilizes a pump-probe measurement, where a single fs laser is employed to provide pump and probe pulses and an optical delay line is used to scan the time delay between pump and probe pulses. Usually, lock-in detection and signal modulation by mechanical or electro-optical chopping are performed in the pump-probe measurement. The AOS was used for time-resolved pump-probe spectroscopy in 1987 [20, 21], where two fs lasers provided pump and probe pulses at different repetition frequencies so that the time delay between the pump and probe pulses was scanned with no use of a mechanical delay line. Also, THz-TDS using AOS has been demonstrated by use of fs lasers at a repetition frequency of 82.6 MHz and 1 GHz [14,15]. In the AOS THz-TDS, one fs laser gives pump pulses to generate THz pulses, and the other gives probe pulses to optically sample the THz pulses. The time delay is repetitively scanned at a difference frequency ($\Delta f = f_{r1} - f_{r2}$), where the f_{r1} and f_{r2} are stabilized repetition frequencies of fs lasers, as shown in Fig. 1(a). In our system, the repetition frequency of pump pulses (f_{r1}) is fixed at 100 MHz. Detailed specifications of our system will be given in Section III. The real time can be converted into the time delay by using

$$\tau(\text{time delay}) = t(\text{real time}) \times \frac{\Delta f}{f_{r1}}. \quad (1)$$

Since the time scaling factor ($\Delta f / f_{r1}$) is on the order of magnitude of 10^{-7} for our system, time-domain data of THz pulses can be acquired at a RF sampling rate by using a digital oscilloscope or digitizer.

2. TFCS

Figure 1(b) describes the principle of the TFCS in the frequency domain. Optical pulses from two fs lasers consist of optical modes whose frequencies are represented as

$$\begin{aligned} f_1 &= nf_{r1} + f_{o1} \\ f_2 &= nf_{r2} + f_{o2} \end{aligned}, \quad (2)$$

where f_{r1} and f_{r2} are stabilized repetition frequencies, f_{o1} and f_{o2} are carrier-envelop offset frequencies, and n is an integer. Optical pulses from the fs laser 1 generate a THz frequency comb from a THz emitter, and those from the fs laser 2 generate photocarrier pulses in a THz detector. The THz frequency comb and photocarrier pulses are represented as

$$\begin{aligned} f_1 &= mf_{r1} \\ f_2 &= mf_{r2} \end{aligned}, \quad (3)$$

where m is an integer. In a THz detector, photocurrent pulses are induced by the photocarrier pulses and the electric field of the THz frequency comb, which are represented as

$$f = m(f_{r1} - f_{r2}) = m\Delta f \quad (4)$$

From Eqs. (3) and (4), the spectrum of the photocurrent pulses can be viewed as the spectrum of the THz frequency comb downscaled by a factor of $\Delta f / f_{r1}$ and can be directly measured using a RF spectrum analyzer. That is, the spectrum of a THz frequency comb can be measured by using multifrequency-heterodyne detection.

III. EXPERIMENTAL SETUPS

1. AOS THz-TDS

Our experimental setup for AOS THz-TDS is sketched in Fig. 2(a). We employ a laser system where the two

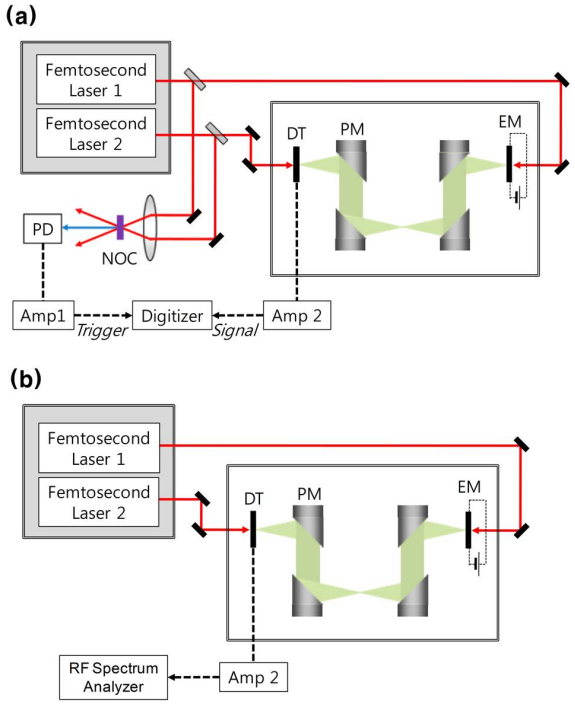

Fig. 2. (a) Our experimental setup for AOS THz-TDS, (EM: THz emitter, DT: THz detector, PM: off-axis parabolic mirror, PD: photodetector, Amp1: current amplifier, Amp 2: variable-gain current amplifier, NOC: nonlinear optical crystal). (b) Our experimental setup for TFCS.

fs lasers with repetition frequencies around 100 MHz are pumped by a diode-pumped solid state laser at a 532-nm wavelength. The whole laser system is placed on a temperature-controlled baseplate to avoid thermal fluctuations. The fs lasers have a center wavelength of 800 nm, and the pulse durations of fs lasers 1 and 2 are 10 and 20 fs, respectively. The repetition frequencies of the fs lasers are, respectively, stabilized by using two phase-locked loops to reduce the time jitter of the optical pulses, as explained below. We use two low-temperature-grown GaAs photoconductive antennas, one as a THz emitter (EM) and the other as a detector (DT).

Optical pulses from the fs laser 1 are incident on the EM to generate THz pulses, which are guided into the DT by using four off-axis parabolic mirrors. Optical pulses from the fs laser 2 are used to optically sample the THz pulses incident upon the DT. A photocurrent output from the DT represents the magnitude of the electric field of the THz pulses temporally sampled. It is amplified by using a variable-gain current amplifier and is then input to a 24-bit flexible resolution digitizer (National Instruments PXI-5922). The digitizer is triggered by a sum-frequency signal generated from a nonlinear optical crystal (2-mm-thick BBO crystal) on which optical pulses from the two fs lasers are non-collinearly focused. The trigger signal has a repetition frequency equal to the difference frequency. We can acquire time-domain data by using the digitizer, and we can average repetitive scans to enhance the signal-to-noise ratio (SNR). The time axis of the time-domain data is converted from a real time to a time delay according to Eq. (1); then, a THz spectrum is obtained by Fourier-transforming the time-domain data.

2. TFCS

Figure 2(b) depicts our experimental setup for TFCS, which is the same as that for AOS THz-TDS except for the data acquisition part. A THz frequency comb generated from the EM by using repetition- frequency-stabilized optical pulses is incident upon the DT via four off-axis parabolic mirrors. Through multifrequency-heterodyne detection, the spectrum of a THz frequency comb is measured with a RF spectrum analyzer (Agilent Technologies N9020A-526), as explained in Section II,

3. Stabilization of Repetition Frequencies

We use two phase-locked loops to stabilize the repetition frequencies of the fs lasers. A schematic diagram of the phase-locked loops is displayed in Fig. 3(a). f_{r1} and f_{r21} are phase-locked to a fixed frequency of 100 MHz and a variable frequency, respectively, so that the difference frequency can be adjusted. By using double-balanced mixers (DBM), the tenth harmonics of f_{r1} and f_{r2} are compared with the outputs of a 1-GHz dielectric resonator oscillator (DRO) and a signal generator (Agilent Technologies N5181A), respectively. The DRO and the signal generator share a 10-MHz reference oscillator to reduce the relative time jitter between optical pulses from the two fs lasers. The phase error signal output from the DBM is amplified by using a proportional-integral amplifier (PI Amp) and a high-voltage amplifier (HV Amp) and is supplied to a piezoelectric transducer (PZT) to which a cavity mirror is attached. The repetition frequencies are stabilized by controlling the cavity lengths via the PZTs.

To evaluate stabilization performance of the phase-locked loops, we performed optical cross-correlation measurements, where a sum-frequency signal is generated from a nonlinear optical crystal (2-mm-thick BBO crystal) on which optical pulses from the two fs lasers are non-collinearly focused. Figure 3(b) shows optical cross-correlation results obtained when the difference frequency is set to 100 Hz and the sum-frequency signal is detected by a photodetector with a bandwidth of 12.5 MHz. As shown by the blue line, a single scan of cross-correlation has a full width at half maximum (FWHM) of 107 fs, which results from broadening of the optical pulse due to dispersion and the response time of the photodetector. The black line displays a cross-correlation signal

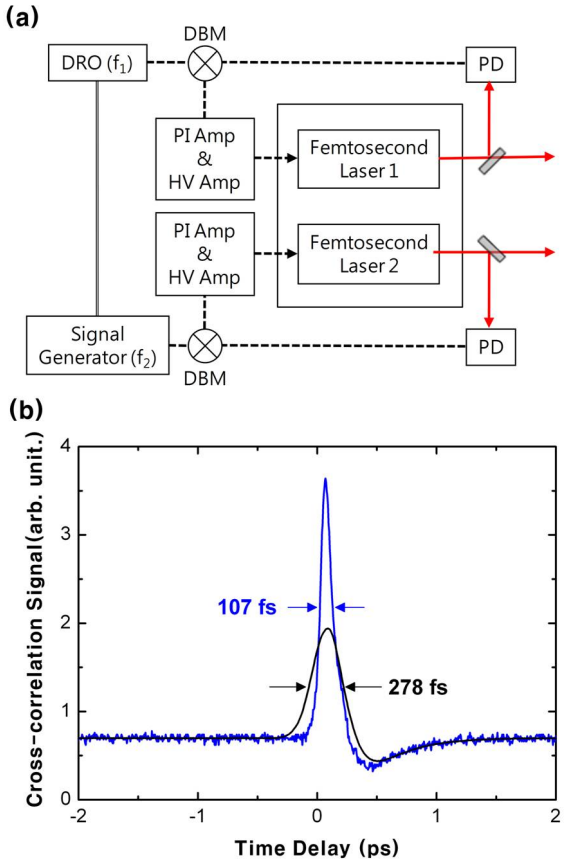

Fig. 3. (a) A schematic diagram of the phase-locked loops; optical paths are represented by red solid lines and electrical signals by black dashed lines, (DRO: dielectric resonator oscillator, DBM: double-balanced mixer, PI Amp: proportional-integral amplifier, HV Amp: high-voltage amplifier, PD: photodetector). (b) A single-scan cross-correlation signal (blue line) between the two fs lasers using non-collinear sum-frequency generation and a cross-correlation signal averaged over 1000 scans (black line).

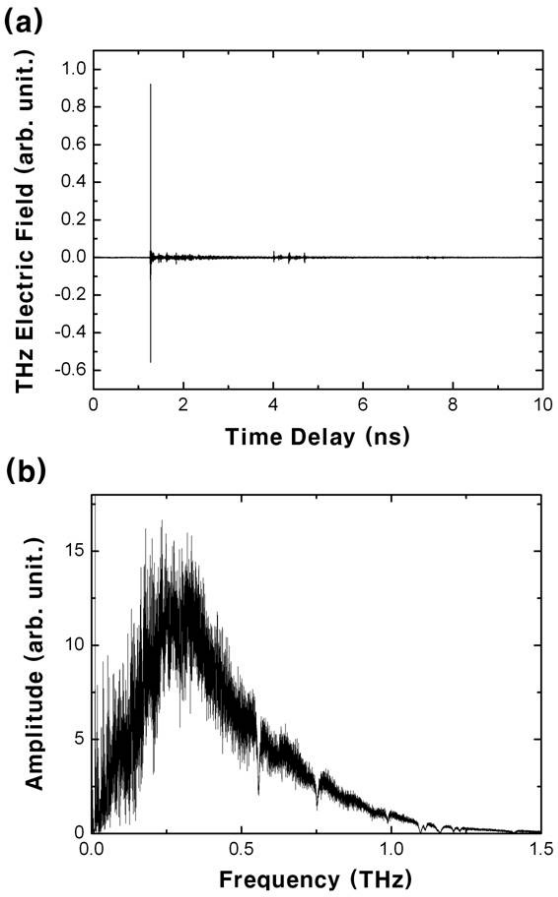

Fig. 4. (a) A typical time-domain waveform on a 10-ns time window measured from AOS THz-TDS. (b) THz spectrum obtained by using a FFT of the time-domain waveform in (a).

averaged over 1000 repetitive scans of the adjacent pulse 10 ms apart from the trigger pulse. It shows a FWHM of 278 fs, which is wider than the FWHM of a single scan and is caused by the relative timing jitter between the optical pulses from the two fs lasers. The time resolution of our system can be taken to be 278 fs.

IV. RESULTS & DISCUSSION

1. AOS THz-TDS

Typical time-domain data on a 10-ns time window measured from AOS-THz TDS are shown in Fig. 4(a). With a difference frequency of 20 Hz, these time domain data are acquired by averaging 1,000 repetitive scans during a measurement time of 100 s. In Fig. 4(b), the THz spectrum obtained by fast Fourier transformation (FFT) of the time-domain data has a frequency resolution of 100 MHz, the inverse of 10 ns. The spectrum has a band of approximately 0.1 $\sim$ 1.5 THz, as can be better seen with the vertical axis on a log scale.

Significant characteristics of this spectrometer are its measurement time, SNR, spectral bandwidth, and spectral resolution. This spectrometer can have a spectral resolution down to 100 MHz, corresponding to the repetition frequency of the fs lasers. In terms of measurement time, SNR, and spectral bandwidth, we tried to find optimal conditions for the difference frequency, a set of parameter for the variable-gain current amplifier, and a sampling rate for the digitizer. When the measurement time was fixed at 100 sec, the set of parameters for the current amplifier was adjusted to keep the virtual spectral bandwidth above 1 THz, and the sampling rate of the digitizer was adjusted to keep a minimum time delay step of 100 fs, we investigated the SNR for various difference frequencies. We define a virtual spectral bandwidth as

$$SB = AB\frac{f_{r1}}{\Delta f}, \tag{5}$$

Table 1. Measurement conditions under which the results of Fig. 5 were obtained.

Difference frequency (Hz)		1	2	5	10	20	50	100
Measurement time (sec)					100			
# of averaged scans		50	100	250	500	1000	2500	5000
Variable-gain current amplifier	Bandwidth (MHz)	0.22	0.22	0.22	0.22	0.22	1.8	1.8
	Gain (V/A)	10^7	10^7	10^7	10^7	10^7	10^6	10^6
Virtual spectral bandwidth (THz)		22	11	4.4	2.2	1.1	3.6	1.8
Digitizer	Sampling rate (MS/sec)	0.1	0.2	0.5	1	2	5	10
	Vertical resolution (bits)	24	24	24	22	20	20	18
Recording length	(minimum time delay step (fs))			10^5		(100)		

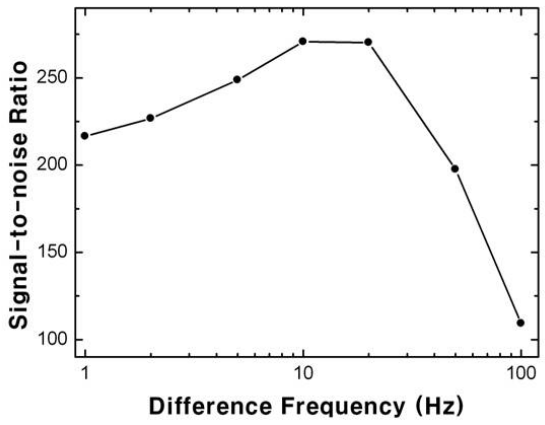

Fig. 5. SNR versus difference frequency.

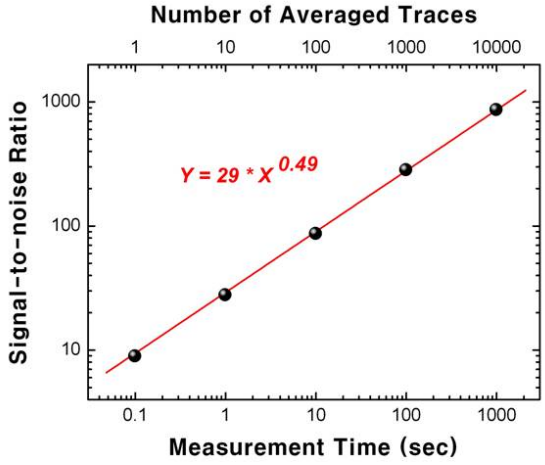

Fig. 6. (color online)SNR versus measurement time. The red line is a fit to the data in the form of Y=α^*X$^{\beta}$.

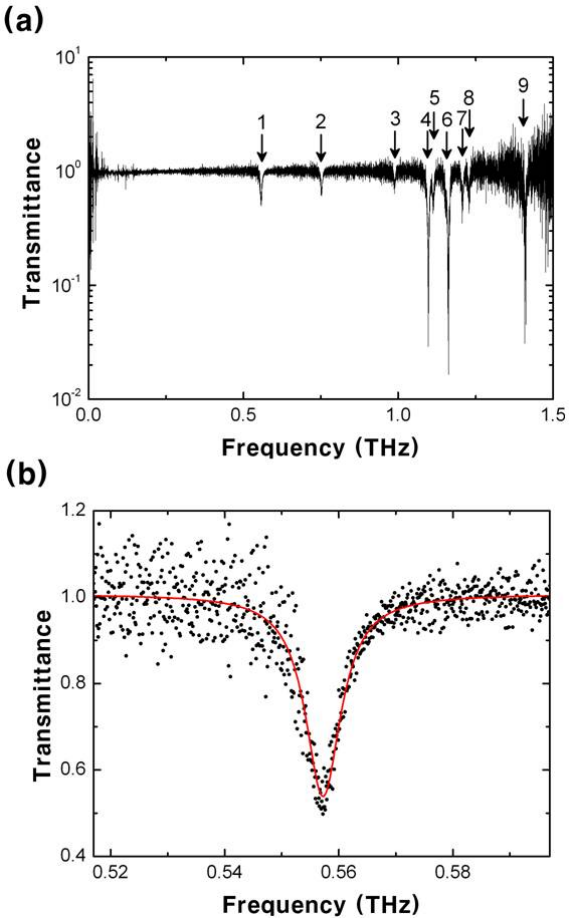

Fig. 7. (color online) (a) THz transmittance spectrum of water vapor. (b) Experimental data (black dot) and its Lorentz fit (red line) with respect to the absorption line 1 of water vapor.

where SB is a virtual spectral bandwidth and AB is the bandwidth of the current amplifier. Figure 5 shows the SNR versus the difference frequency, and the measurement conditions under which the results of Fig. 5 are obtained are given in Table 1. We obtain the highest SNR at a difference frequency of 10∼20 Hz, as shown in Fig. 5. It should be noted that the scan rate is equivalent to half the difference frequency in our measurements. When the digitizer was triggered by a trigger pulse, it acquired data during the entire time interval between the trigger pulse and the next one so that it could not be triggered by the next one. As a result, the dead time amounts to half the measurement time. For example, a scan rate of 10 Hz is obtained at a difference frequency

Table 2. Absorption lines of water vapor in the frequency range from 0.1 to 1.5 THz.

	Frequency (GHz)	Linewidth (GHz)
1	557.2	7.6
2	752.3	6.8
3	987.9	6.8
4	1097.3	10.1
5	1113.0	5.9
6	1160.9	14.1
7	1207.7	7.7
8	1228.9	4.7
9	1410.2	9.8

of 20 Hz.

Also, we investigated the relation between the SNR and the measurement time. Figure 6 shows the variation in the SNR with measurement time, which was measured at a difference frequency of 20 Hz. The SNR increases from 9 to 860 as the measurement time increases from 0.1 sec to 1000 sec. The red line is a fit to the data in the form of $Y = \alpha^* X^\beta$, where X is the measurement time and Y is the SNR. When the system noise is limited by the shot noise, the value of β is expected to be close to 0.5. Therefore, the noise level of our system for the AOS THz-TDS is confirmed to be close to the shot noise limit.

Using our system for AOS THz-TDS, we investigated the THz transmission of water vapor. Figure 7(a) shows a THz transmittance spectrum of water vapor obtained from THz spectra at a relative humidities of 35 and 5% at 21.5^0C. Nine absorption lines of water vapor are shown in the frequency range of $0.1 \sim 1.5$ THz. The absorption lines were analyzed assuming a Lorentzian line shape, and the central frequencies and the linewidths of the lines are given in Table 2. As an instance, Fig. 7(b) shows a Lorentz fit of the absorption line 1 at 557.2 GHz. We also confirm that the measured results are in good agreement with previous ones [22].

2. TFCS

In contrast with AOS THz-TDS where a time-domain data are measured with a digitizer and a FFT should be performed to obtain a spectrum, we can directly measure the THz spectrum by using a RF spectrum analyzer, instead of a digitizer, in TFCS. A trigger signal for data acquisition, as well as a FFT of a time-domain data, is not needed. A typical THz spectrum obtained from a single sweep is shown in Fig. 8(a), which was measured with a resolution bandwidth (RBW) of 20 Hz and a video bandwidth (VBW) of 20 Hz during a measurement time of 907 sec. Because the difference frequency and the number of data points are set to 20 Hz and 15000, respectively, the spectrum has a frequency resolution of 100 MHz. It is almost similar to the spectrum (Fig. 4(b)) measured from AOS THz-TDS, and the absorption lines of water vapor can be also seen. The SNR of the spectrum is estimated to be 10. In addition, individual comb modes can be clearly resolved in the spectrum.

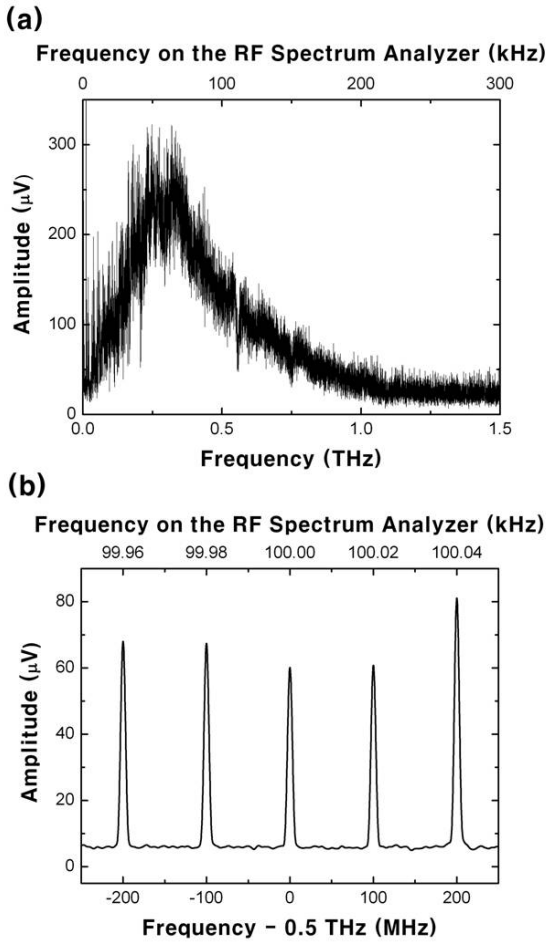

Fig. 8. (a) Typical spectrum measured from TFCS. (b) THz frequency comb modes are clearly resolved at around 0.5 THz.

Figure 8(b) shows a spectrum with a span of 500 MHz at around 0.5 THz, which is obtained by averaging 100 traces for a measurement time of 180 sec with a RBW of 1 Hz and a VBW of 1 Hz. It is shown that the comb modes have frequencies of multiples of the repetition frequency (100 MHz), as described in Eq.(3). TFCS will be able to be used for high-accuracy THz frequency metrology. However, it should be noted that AOS THz-TDS has an advantage over TFCS in terms of SNR and needs a shorter measurement time than TFCS to attain a specific SNR.

V. CONCLUSION

In conclusion, we have demonstrated and characterized two types of high-speed high-resolution THz spectrometers. We showed that our system for AOS THz-TDS had a time resolution of 278 fs and that its noise level was close to the shot noise limit. The THz transmittance spectrum of water vapor was measured using the AOS THz-TDS. Both AOS THz-TDS and TFCS have a frequency resolution of 100 MHz. Although TFCS is simpler experimentally and for data acquisition; AOS THz-TDS enables a more rapid measurement. The spectrometers will be able to be widely used as powerful spectroscopic and metrological tools in the THz field.

ACKNOWLEDGMENTS

This work was supported in part by the IT R&D program of MKE/IITA [2008-F-021-01] and in part by the Ministry of Education, Science, and Technology through the project KRISS-09011005.

REFERENCES

[1] K. Liu, J. Xu, T. Yuan and X.-C. Zhang, Phys. Rev. B **73**, 155330 (2006).
[2] M. Yi, K. Lee and J. Ahn, J. Korean Phys. Soc. **51**, 475 (2007).
[3] M. Yi, K. H. Lee, I. Maeng, J. H. Son, R. D. Averitt and J. Ahn, Jpn. J. Appl. Phys. **47,** 202 (2008).
[4] N. E. Yu, C. Jung, C. S. Kee, Y. L. Lee, B. A. Yu, D. K. Ko, J. Lee, W. J. Lee, J. E. Kim and H. Y. Park, J. Korean Phys. Soc. **51**, 493 (2007).
[5] H. T. Chen, W. J. Padilla, J. M. O. Zide, A. C. Gossard, A. J. Taylor and R. D. Averitt, Nature **444**, 597 (2006).
[6] J. Ahn, A. V. Efimov, R. D. Averitt and A. J. Taylor, Opt. Express **11**, 2486 (2003).
[7] B. B. Jin, P. Kuzel, F. Kadlec, T. Dahm, J. M. Redwing, A. V. Pogrebnyakov, X. X. Xi and N. Klein, Appl. Phys. Lett. **87**, 092503 (2005).
[8] F. N. Keutsch, M. G. Brown, P. B. Petersen, R. J. Saykally, M. Geleijns and A. V. D. Avoird, J. Chem. Phys. **114**, 3994 (2001).
[9] C. Kistner, A. Andre, T. Fischer, A. Thoma, C. Janke, A. Bartels, T. Gisler, G. Maret and T. Dekorsy, Appl. Phys. Lett. **90**, 233902 (2007).
[10] B J. Ahn, D. N. Hutchinson, C. Rangan and P. H. Bucksbaum, Phys. Rev. Lett. **86**, 1179 (2001).
[11] B. E. Cole, J. B. Williams, B. T. King, M. S. Sherwin and C. R. Stanley, Nature **410**, 60 (2001).
[12] G. Kim, S. Jeon, J. Kim and Y. Jin, Rev. Sci. Instrum. **79**, 106102 (2008).
[13] H. Hoshina, T. Seta, T. Iwamoto, I. Hosako, C. Otani and Y. Kasai, J. Quant. Spectrosc. Radiat. Transfer **109,** 2303 (2008).
[14] T. Yasui, E. Saneyoshi and T. Araki, Appl. Phys. Lett. **87**, 061101 (2005).
[15] C. Janke, M. Forst, M. Nagel, H. Kurz and A. Bartels, Opt. Lett. **30**, 1405 (2005).
[16] A. Bartels, A. Thoma, C. Janke, T. Dekorsy, A. Dreyhaupt, S. Winnerl and M. Helm, Opt. Express **14**, 430 (2006).
[17] A. Bartels, R. Cerna, C. Kistner, A. Thoma, F. Hudert, C. Janke and T. Dekorsy, Rev. Sci. Instrum. **78**, 035107 (2007).
[18] T. Yasui, Y. Kabetani, E. Saneyoshi, S. Yokoyama and T. Araki, Appl. Phys. Lett. **88**, 241104 (2006).
[19] S. Yokoyama, R. Nakamura, M. Nose, T. Araki and T. Yasui, Opt. Express **16**, 13052 (2008).
[20] P. A. Elzinga, F. E. Lytle, Y. Jian, G. B. King and N. M. Laurendeau, Appl. Spectrosc. **41**, 2 (1987).
[21] P. A. Elzinga, R. J. Kneisler, F. E. Lytle, Y. Jiang, G. B. King and N. M. Laurendeau, Appl. Opt. **26**, 4303 (1987).
[22] M. van Exter, C. Fattinger and D. Grischkowsky, Opt. Lett. **14**, 1128 (1989).